



Synthesis and Characterization of Hematite (α - Fe_2O_3) Nanomaterials from Red Mud Using EDTA as Capping Agent

Berlian Sitorus ^{1,*}, Yunior Arta Arga Manulang ¹, Risyas Sasri ¹, Seno D. Panjaitan ²

¹ Department of Chemistry, Faculty of Mathematics and Natural Sciences, Universitas Tanjungpura, Pontianak, West Kalimantan, Indonesia

² Department of Electrical Engineering, Faculty of Engineering, Universitas Tanjungpura, Pontianak, West Kalimantan, Indonesia

* Corresponding author: berlian.sitorus@chemistry.untan.ac.id

<https://doi.org/10.14710/jksa.28.8.463-469>



Article Info

Article history:

Received: 09th July 2025

Revised: 28th October 2025

Accepted: 29th October 2025

Online: 31st October 2025

Keywords:

Capping agent; EDTA; Hematite nanomaterial; Iron Oxide; Red Mud

Abstract

Hematite (α - Fe_2O_3) nanomaterials, a stable phase of iron oxide, hold significant potential for diverse materials science and technology applications. In this study, red mud was employed as a low-cost precursor for synthesizing hematite nanomaterials, with ethylenediaminetetraacetic acid (EDTA) used as a capping agent to prevent particle agglomeration. The effect of EDTA on particle size and colloidal stability was investigated by comparing three synthesis variations: (a) without EDTA (NPH-1), (b) with EDTA via the precipitation method (NPH-2), and (c) with EDTA via the hydrothermal method (NPH-3). XRD analysis confirmed the formation of crystalline hematite (α - Fe_2O_3) in all samples. FT-IR spectroscopy revealed absorption bands at 1624 cm^{-1} and 1382 cm^{-1} , corresponding to the symmetric and asymmetric stretching vibrations of the carboxylate (COO^-) group, respectively. The difference in these wavenumbers suggests monodentate coordination between the carboxyl groups of EDTA and the hematite nanoparticle surfaces. Particle size analysis indicated that the EDTA-assisted synthesis via precipitation (NPH-2) produced the smallest average particle size (149.6 nm) with a narrow size distribution, as reflected by a polydispersity index (PDI) of 0.43. Furthermore, this sample demonstrated enhanced colloidal stability with a zeta potential of -34.0 mV . These findings suggest that the synthesized α - Fe_2O_3 nanomaterials produced with narrow particle size distribution and high colloidal stability, are promising for visible-light photocatalysis.

1. Introduction

Nanomaterials are materials that possess external dimensions or internal structures on the nanoscale. The synthesis of nanomaterials is driven by the goal of achieving unique physicochemical properties that differ significantly from their bulk counterparts, enabling advanced functionalities in various applications [1]. Among metal oxide nanomaterials, hematite (α - Fe_2O_3) has attracted considerable attention due to its broad applicability in catalysis, electrochemical devices, gas sensing, pigments, magnetic materials, clinical therapy, and diagnostics. Hematite is one of the stable crystalline phases of iron(III) oxide, alongside maghemite (γ - Fe_2O_3) [2]. It crystallizes in a rhombohedral structure, which is often described as a hexagonal close-packed (hcp) arrangement (Figure 1), with lattice parameters of $a =$

0.5034 nm and $c = 1.375\text{ nm}$ [3]. Hematite nanomaterials can be synthesized from various iron-rich sources, including iron sand residues [4] and red mud, a byproduct of alumina production [5].

Red mud is a solid industrial waste generated as a byproduct of the Bayer process, which is used for extracting alumina from bauxite ore. For every ton of alumina produced, approximately 0.8 to 1.5 tons of red mud are generated [5]. The disposal of red mud presents serious environmental challenges, particularly regarding soil degradation and water contamination [6]. To mitigate these environmental impacts, one promising strategy is the recovery and utilization of valuable metal oxides contained within red mud. Notably, red mud is rich in iron content, typically containing around 30.448% iron oxide (Fe_2O_3) [7].

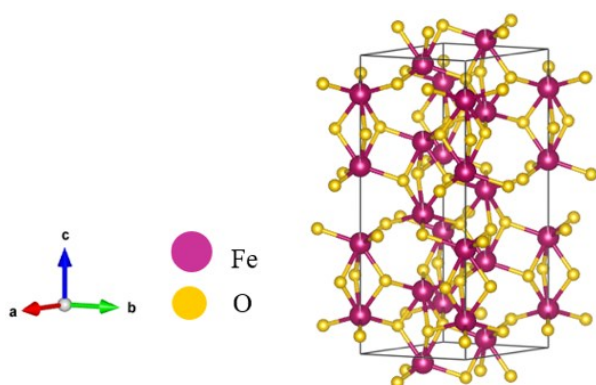


Figure 1. Crystal structure of hematite ($\alpha\text{-Fe}_2\text{O}_3$), showing the rhombohedral arrangement of Fe^{3+} and O^{2-} ions [8]

Hematite nanomaterials can be synthesized through precipitation and hydrothermal methods, both are widely used due to their simplicity, cost-effectiveness, and relatively short processing times. The precipitation method involves the controlled addition of a precipitating agent into a metal ion solution, allowing the formation of solid particles as the pH of the solution is carefully adjusted. The resulting precipitate is typically subjected to a subsequent calcination step to obtain the desired crystal structure and morphology. The hydrothermal method facilitates solid-state reactions in an aqueous medium within a sealed autoclave under elevated temperature and pressure, promoting the formation of fine-grained particles [9].

One of the key factors in the successful synthesis of hematite nanomaterials is the selection of an appropriate capping agent. Due to their high surface energy, nanoscale hematite particles are prone to agglomeration, which can result in increased particle size and reduced functionality. Therefore, a suitable capping agent is crucial for controlling particle growth, preventing agglomeration, and enhancing particle stability [8].

Capping agents are crucial in stabilizing nanoparticles by forming a protective surface layer that prevents interparticle interactions and limits further growth [8]. This stabilization can occur through two primary mechanisms. First, the functional groups present in the capping agent can chemically interact (either through covalent or non-covalent bonding) with the nanoparticle surface, thereby passivating and stabilizing it. Second, capping agents with ionic (cationic or anionic) properties can promote electrostatic repulsion between nanoparticles, effectively minimizing aggregation and enhancing colloidal stability [10].

In this study, ethylenediaminetetraacetic acid (EDTA) was employed as a capping agent for synthesizing hematite nanoparticles due to its well-established safety, biocompatibility, and strong metal chelating properties. With two amine and four carboxyl groups, EDTA binds strongly to iron cations on the nanoparticle surface [11, 12], enhancing colloidal stability, lowering surface energy, and preventing agglomeration during and after synthesis [11, 13]. This study uniquely explores the role of EDTA as a capping agent in controlling the formation and stability of $\alpha\text{-Fe}_2\text{O}_3$ derived from red mud, employing two

different synthesis routes, precipitation and hydrothermal, which have not been previously reported.

2. Experimental

2.1. Materials and Instrumentation

The materials employed in this research were water (H_2O), ethylenediaminetetraacetic acid (EDTA) (Sigma Aldrich, Germany), hydrochloric acid (HCl) 37% (Merck 258148), nitric acid (HNO_3) 65% (Merck 438073), sodium hydroxide (NaOH) (Merck 106498), and red mud from the bauxite residue site of PT. Indonesia Chemical Alumina (ICA), located in Tayan District, Sanggau Regency, West Kalimantan. The instruments used to characterize hematite nanoparticles were X-ray Fluorescence (XRF; PANalytical Epsilon 3), Fourier Transform Infrared Spectroscopy (FT-IR; SHIMadzu), X-ray Diffraction (XRD; Bruker D8 Advance), and Particle Size Analyzer (PSA; Horiba SZ-100).

2.2. Pretreatment of Red Mud

The red mud powder (Figure 2(a)) was pretreated by dissolving the material in 0.3 M HCl, maintaining a solid-to-liquid ratio of 1:20 (w/v), and stirring continuously using a magnetic stirrer at 40°C for 2 hours. Afterward, the mixture was filtered, and the solid residue was thoroughly washed multiple times with deionized water to eliminate residual acid and soluble contaminants. The washed solid was dried in a conventional oven at 105°C for 12 hours. The washing step aimed to eliminate impurities such as calcium, silica, and aluminum from the red mud matrix [6]. The washed solid (Figure 2(b)) was then subjected to magnetic separation using a neodymium magnet to isolate magnetically responsive particles from non-magnetic fractions [14]. The magnetic fraction was ground and sieved through a 200 mesh sieve to obtain a fine and uniform powder (Figure 2(c)).

2.3. Extraction Process

The magnetically separated sample from the previous step was leached in 3 M HCl (w/v ratio of 1 g/20 mL). The mixture was stirred and refluxed at 95°C for 2 hours to enhance metal dissolution. Upon cooling to room temperature, the solution was filtered, and the resulting yellow filtrate (Figure 3) (indicative of the presence of Fe^{3+} ions) was collected [15]. To recover iron from the acidic solution, 4 M NaOH was gradually added to the filtrate until the pH reached 13, promoting the selective precipitation of iron while effectively separating it from aluminum and other metallic impurities [5, 6]. The resulting precipitate was then collected and dried in an oven at 105°C for 12 hours.

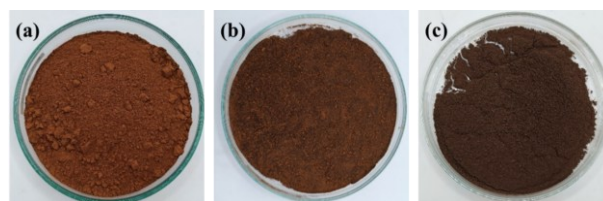


Figure 2. (a) Red mud powder, (b) Red mud powder after washing with 0.3 M HCl, (c) Magnetically separated solid (red mud after washing with 0.3 M HCl)

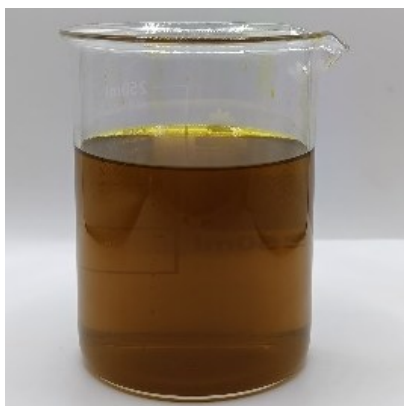


Figure 3. Yellow filtrate obtained after dissolving the magnetically separated red-mud solid in 0.3 M HCl

2.4. Synthesis of Hematite Nanomaterial

The solid obtained from the previous step was dissolved in 3 M HNO₃ at a solid-to-liquid ratio of 1 g/20 mL and stirred for approximately 30 minutes. Subsequently, 4 M NaOH was added dropwise until the pH reached 11. The mixture was then stirred and refluxed at 95°C for 4 hours. The precipitate was filtered, thoroughly washed with distilled water, and dried in an oven at 80–90°C for 12 hours. Finally, the dried solid was calcined at 600°C for 2 hours, yield the product, labeled as NPH-1.

For the synthesis of the second sample, the same initial procedure was followed: the dried solid was dissolved in 3 M HNO₃ (1 g/20 mL) and stirred for 30 minutes. Then, 4.8 g of EDTA and 4 M NaOH solution were added until the pH reached 11. The mixture was refluxed at 95°C for 4 hours. After cooling, the precipitate was filtered and thoroughly washed with deionized water. The resulting solid was divided into two portions. The first portion (precipitate A) was dried in an oven at 80–90°C for 12 hours and calcined at 600°C for 2 hours, yielding the product labelled NPH-2. The second portion (precipitate B) was subjected to hydrothermal treatment at 180°C for 12 hours. The obtained solid was dried at 80–90°C for 12 hours and calcined at 600°C for 2 hours. The final product was designated as NPH-3. This study identified the capping agent as a critical parameter due to its essential role in preventing particle agglomeration and enhancing surface stabilization.

2.5. Characterization

The crystalline phase of hematite nanomaterials for each treatment was characterized using XRD. The instrument is operating at 40.0 kV and 15 mA, with sample scanning conducted at a rotation speed of 10°/min over a 2θ range of 10°–90°. The functional groups of EDTA interacting with the surface of the hematite nanomaterials were identified using FT-IR spectroscopy, employing KBr pellets within the wavenumber range of 4000–400 cm⁻¹. Lastly, the particle size of the hematite nanomaterials was determined using a PSA. For PSA measurements, the samples were prepared by dispersing hematite nanoparticles in 100 mL of distilled water at a concentration of 1000 ppm, followed by sonication for 90 minutes [16].

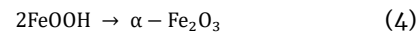
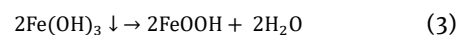
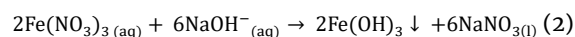
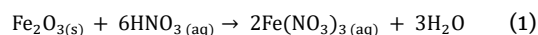
3. Results and Discussion

3.1. Preparation of Red Mud

This study employed red mud as the primary raw material for synthesizing hematite nanomaterials. The red mud was analyzed using XRF spectroscopy to determine its chemical composition. The results, summarized in Table 1, revealed that the red mud is predominantly composed of Fe₂O₃, confirming its suitability as a precursor for hematite synthesis.

3.2. Synthesis of Hematite Nanomaterial

The synthesis of hematite nanomaterials was done through a two-step process: (1) the dissolution of precursor solids to produce Fe³⁺ ions, and (2) the subsequent precipitation of iron hydroxide. HNO₃ was employed as the leaching agent to dissolve the iron-containing compounds (Equation 1), while NaOH was gradually added to the solution until the pH reached 11. The addition of NaOH led to the formation of a reddish-brown precipitate, indicating the successful precipitation of ferric hydroxide (Fe(OH)₃) (Equation 2) [17]. This precipitate was then subjected to a drying process (Equation 3), followed by calcination to induce phase transformation into crystalline hematite (α-Fe₂O₃) (Equation 4) [18].



The synthesis of hematite nanomaterials with a capping agent was performed by incorporating EDTA into the reaction system, followed by gradually adding NaOH until the solution reached a pH of 11. At this pH, NaOH not only facilitates the precipitation of Fe³⁺ ions as Fe(OH)₃ (Equation 1) but also promotes the deprotonation of EDTA's four carboxyl groups, enhancing their ability to chelate metal ions. This deprotonation is supported by the fourth dissociation constant (pK_{a4}) of EDTA, which is 10.26 [19]. The deprotonated carboxyl groups, along with the amine functionalities of EDTA, coordinate with Fe³⁺ ions on the surface of the hematite nanoparticles. This coordination results in the formation of a shell or coating around the particles. This interaction stabilizes the nanoparticles by preventing agglomeration, thereby effectively restricting further particle growth and maintaining a uniform nanoscale size distribution.

Table 1. Composition of several elements and compounds of the red mud

Element	% Relative weight	Oxide compounds	% Relative weight
Fe	21.5	Fe ₂ O ₃	30.7
Al	10.3	Al ₂ O ₃	19.5
Si	7.79	SiO ₂	17
Ti	1.47	TiO ₂	2.45
Ca	0.86	CaO	1.21

3.3. Fourier transform Infrared (FT-IR)

Figure 4 presents the FT-IR spectra of the synthesized hematite nanomaterials, both with and without EDTA. In the spectrum of the NPH-1 sample (synthesized without EDTA), Fe-O stretching vibrations are observed at wavenumbers 646 cm⁻¹, 559 cm⁻¹, and 468 cm⁻¹, consistent with characteristic hematite. Fe-O vibrations are also present for the EDTA-modified samples, appearing at 624 cm⁻¹ and 451 cm⁻¹ in NPH-2, and at 559 cm⁻¹ and 476 cm⁻¹ in NPH-3 [11, 20]. The broad absorption bands around 3427 cm⁻¹, 3423 cm⁻¹, and 3421 cm⁻¹ in NPH-1, NPH-2, and NPH-3, respectively, are attributed to O-H stretching vibrations, indicating the presence of hydroxyl groups. Additionally, a band at 3014 cm⁻¹ corresponds to C-H stretching [21].

The FT-IR spectrum of EDTA shows a peak at 968 cm⁻¹ corresponding to C-C stretching, along with peaks at 1010 cm⁻¹ and 1317 cm⁻¹, which are attributed to N(-CH₂-)₃ stretching and CH₂ wagging within the amine groups, respectively [11, 21, 22]. A prominent peak at 1415 cm⁻¹ arises from C-O stretching, while the sharp band at 1695 cm⁻¹ is assigned to the C=O stretching of the carboxylic acid (-COOH) group in uncoordinated EDTA [21, 23].

Notably, the absorption band at 1695 cm⁻¹ may disappear or shift because of the deprotonation of carboxylic groups in EDTA. Upon deprotonation, these groups form carboxylate ions exhibiting symmetric stretching (V_s) and asymmetric stretching (V_{as}). The difference in wavenumber between these two (ΔV = V_{as}-V_s) modes provides insight into the coordination type. If a carboxylate ligand coordinates with surface hematite in a bidentate mode, then the difference in wavenumber between these two (ΔV) is less than 200 cm⁻¹, whereas for monodentate coordination, the ΔV exceeds 200 cm⁻¹ [24].

In the FT-IR spectrum of the NPH-2 sample, absorption peaks at 1382 cm⁻¹ and 1624 cm⁻¹ correspond to the V_s and V_{as} of the carboxylate group (COO⁻), respectively [20, 21]. The wavenumber difference between these peaks (ΔV = 1624-1382 = 242 cm⁻¹) indicates the formation of a coordination complex between the carboxyl groups of EDTA and the hematite nanoparticle surface through monodentate ligand binding. In contrast, these characteristic peaks were absent in the NPH-3 spectrum, suggesting hydrothermal treatment disrupted the interaction between Fe³⁺ ions on the hematite surface and the EDTA molecules. FTIR spectra in Figure 4 show that characteristic organic bands of EDTA (1695, 1415, 1317 cm⁻¹) disappear completely in NPH-3 after calcination at 600°C, leaving only Fe-O lattice vibrations at 559 and 476 cm⁻¹. This confirms that EDTA functioned solely as a chelating agent during synthesis and fully decomposed upon calcination, yielding a stable α-Fe₂O₃ surface free of organic residues.

3.4. X-ray Diffraction (XRD)

Each synthesized material exhibits a distinct, characteristic XRD pattern. XRD analysis was conducted on samples NPH-1, NPH-2, and NPH-3 to verify the formation of the hematite phase, as shown in Figure 5. The XRD patterns of all samples exhibit distinct peaks at

2θ = 24.10°, 33.13°, 35.62°, 40.46°, 49.46°, 54.05°, 62.43°, and 64.02°, which correspond to the crystal planes [012], [104], [110], [113], [024], [116], [214], and [300], respectively. These peaks are consistent with the hematite crystalline phase, as referenced in JCPDS Card No. 33-664 [25]. In diffractogram NPH-2, a distinct peak at 2θ = 29.32° is observed, which is presumed to originate from residual NaNO₃ that was not entirely removed during the water washing process. Furthermore, the synthesized hematite nanomaterials' average crystallite diameter (D) was estimated using the Debye-Scherrer equation (Equation 5).

$$D = \frac{k\lambda}{\beta \cos\theta} \quad (5)$$

Where D is the crystallite diameter, k is the shape factor (k = 0.94), λ is the wavelength of Cu-Kα anode radiation (λ = 1.54 Å), β is the full width at half maximum (FWHM) in radians, and θ is the Bragg diffraction angle [25]. Using the Debye-Scherrer equation, the average crystallite diameters were determined to be 36 nm, 35 nm, and 44 nm for NPH-1, NPH-2, and NPH-3, respectively.

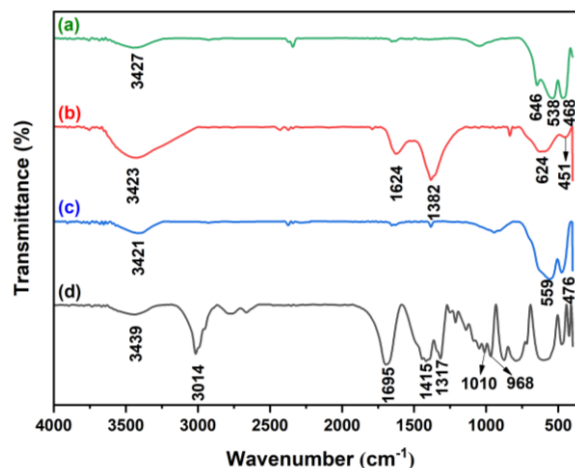


Figure 4. FT-IR spectra of (a) NPH-1 (without EDTA), (b) NPH-2 (with EDTA via the precipitation method), (c) NPH-3 (with EDTA via the hydrothermal method), and (d) EDTA

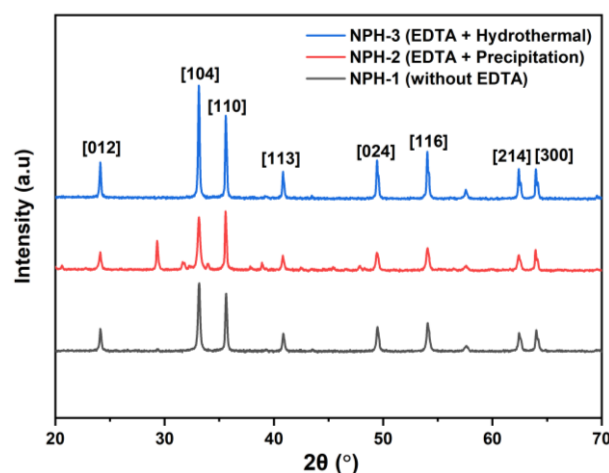


Figure 5. X-ray diffraction patterns of NPH-1, NPH-2, and NPH-3, showing diffraction peaks corresponding to α-Fe₂O₃

3.5. Particle Size Analyzer (PSA)

Based on PSA, the average particle sizes of hematite nanoparticles synthesized without EDTA (NPH-1), with EDTA via the precipitation method (NPH-2), and with EDTA via the hydrothermal method (NPH-3) were 164.1 nm, 149.6 nm, and 162.7 nm, respectively (Table 2 and Figure 6). These values fall within the defined nanoscale range of 1–1000 nm [16], confirming the successful synthesis of nanostructured materials. Among the samples, NPH-2 exhibited the smallest particle size (149.6 nm), indicating that the combination of EDTA as a capping agent and the precipitation method was most effective in limiting particle growth. This result highlights the role of EDTA in inhibiting particle agglomeration, thereby enhancing the stability of hematite nanoparticles.

In the NPH-3 sample (with EDTA via the hydrothermal method), an increase in particle size to 162.7 nm was observed. This increase is likely due to the disruption of interactions between Fe³⁺ ions and EDTA molecules during hydrothermal conditions, as evidenced by the FT-IR spectra shown in Figure 4. The breakdown of Fe-EDTA coordination allows for interparticle interactions, promoting agglomeration and forming larger hematite particles. These findings underscore the critical role of EDTA as a capping agent in inhibiting agglomeration and regulating particle growth under appropriate synthesis conditions.

Table 2. Particle size, PDI, and Zeta potential of NPH-1, NPH-2, and NPH-3

Sample	Particle size (nm)	PDI	Zeta potential (mV)
NPH-1	164.1	0.315	-30.3
NPH-2	149.6	0.436	-34.0
NPH-3	162.7	0.642	-36.4

The polydispersity index (PDI) measures particle size distribution homogeneity, where values below 0.4 indicate a monodisperse or narrow size distribution, while values above 0.4 reflect increasing polydispersity [26]. The PDI values for hematite nanoparticle samples NPH-1 and NPH-2 were 0.315 and 0.436 (Table 2). These findings indicate that NPH-1 and NPH-2 possess a relatively monodisperse particle size distribution. In contrast, sample NPH-3 exhibited a PDI value of 0.642, suggesting a broader and more heterogeneous distribution characteristic.

Zeta potential measurements provide valuable insights into the colloidal stability of hematite nanoparticles in suspension. Higher absolute values of zeta potential, whether positive or negative, reflect stronger electrostatic repulsion between particles, thereby reducing the likelihood of agglomeration and enhancing stability [8]. As presented in Table 2, the zeta potential values for NPH-2 and NPH-3 were -34 mV and -36.4 mV, respectively, both more negative than that of NPH-1 (-30.3 mV). Although these differences are relatively small, they still suggest a slight improvement in surface charge density and electrostatic repulsion, which can enhance short-term dispersion and reduce soft agglomeration during synthesis. The incorporation of EDTA as a capping agent during hematite nanoparticle synthesis thus contributes to better surface charge stabilization, effectively improving the colloidal stability and uniformity of the hematite suspensions [26].

The PSA revealed that the average diameters of the hematite samples (149–164 nm) were larger than the crystallite sizes estimated from XRD (36–44 nm). This commonly occurs in nanostructured oxides due to particle agglomeration in suspension. XRD reflects coherent diffraction domains, whereas PSA measures the hydrodynamic diameter of dispersed particles, which often include soft agglomerates formed by magnetic and surface interactions of α -Fe₂O₃ nanoparticles. Similar observations were reported in previous studies on hematite nanomaterials [26, 27].

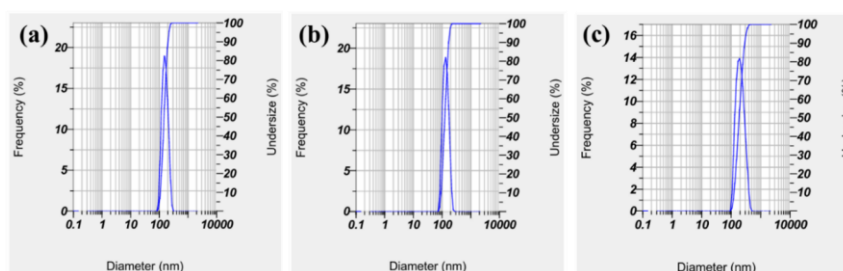


Figure 6. Particle-size distributions of (a) NPH-1, (b) NPH-2, and (c) NPH-3 determined by PSA, indicating the influence of EDTA addition on particle size characteristics

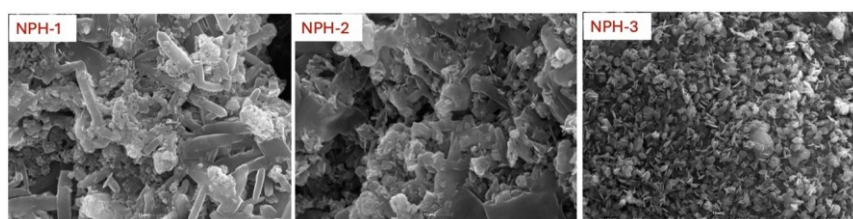


Figure 7. SEM micrographs of α -Fe₂O₃ synthesized from red mud: (a) NPH-1 (without EDTA), (b) NPH-2 (with EDTA via precipitation method), and (c) NPH-3 (with EDTA via hydrothermal method)

Figure 7 presents the SEM images of α -Fe₂O₃ particles synthesized from red mud under different synthesis conditions. In the sample without EDTA (NPH-1), the particles appear as irregular, elongated rods that tend to form large agglomerates, indicating uncontrolled crystal growth. When EDTA was added during the precipitation process (NPH-2), the morphology became denser and slightly more uniform, suggesting that EDTA helped to slow down the growth of Fe³⁺ nuclei through complex formation. A clearer effect is seen in the hydrothermal sample (NPH-3), where the particles are finer, more evenly distributed, and show a nearly spherical or plate-like appearance. The addition of EDTA modifies the particle morphology from irregular, elongated aggregates (a) to smaller and more uniform grains (b-c), indicating its role as a capping and growth-controlling agent during synthesis. This result suggests that EDTA plays an important role as a capping and growth-controlling agent, improving particle dispersion and morphological uniformity.

Compared with previous studies on red-mud-derived hematite, the samples obtained in this work exhibited crystallite sizes of 36–44 nm (XRD) and particle diameters of 149–164 nm (PSA), consistent with secondary agglomerate formation in aqueous suspension. These values are slightly larger than those reported by Chakraborty *et al.* [28], who synthesized α -Fe₂O₃ nanoflakes with smaller crystallites (2.1–16.4 nm) and higher surface areas (136–347 m² g⁻¹). The measured zeta potentials (-30.3 to -36.4 mV) fall within the typical stability threshold ($|\zeta| \geq 30$ mV) [28, 29], confirming that EDTA incorporation enhances surface charge density and dispersion stability. Similar behavior was reported by Mbuyazi and Ajibade [29], where the presence of a capping agent significantly influenced particle morphology and stability. Likewise, the addition of EDTA in this study produced smaller, more uniform α -Fe₂O₃ particles with improved colloidal stability compared to the uncapped sample, demonstrating that EDTA acts effectively as a chelating and capping agent controlling crystal growth and surface charge stabilization.

4. Conclusion

The synthesis of hematite (α -Fe₂O₃) nanomaterials from red mud using EDTA as a capping agent effectively minimized agglomeration and controlled particle growth. Among the samples, NPH-2 (with EDTA via the precipitation method) exhibited the smallest average particle size (149.6 nm), a polydispersity index (PDI) value of 0.436, indicating a narrow particle size distribution, and a high negative zeta potential (-34 mV), reflecting strong colloidal stability. These findings highlight the critical role of EDTA in stabilizing the nanoparticle surface by suppressing uncontrolled nucleation and aggregation. Accordingly, EDTA-assisted synthesis represents a promising approach for tuning the physicochemical characteristics of hematite nanomaterials for advanced technological applications. Overall, this study demonstrates the potential of red mud as a sustainable precursor for producing stable hematite nanoparticles applicable to photocatalysis and environmental remediation.

References

- [1] Vancha Harish, Md Mustafiz Ansari, Devesh Tewari, Manish Gaur, Awadh Bihari Yadav, María-Luisa García-Betancourt, Fatehy M. Abdel-Haleem, Mikhael Bechelany, Ahmed Barhoum, Nanoparticle and Nanostructure Synthesis and Controlled Growth Methods, *Nanomaterials*, 12, 18, (2022), 3226 <https://doi.org/10.3390/nano12183226>
- [2] Amanullakhan Pathan, Sandip H. Bhatt, Shailesh Vajapara, C. P. Bhasin, Solar light induced photo catalytic properties of α -Fe₂O₃ nanoparticles for degradation of methylene blue dye, *International Journal of Thin Film Science and Technology*, 11, 2, (2022), 213-224
- [3] Ahmad Fajri Soekansa, Nafis Sudirman, Syamsi Aini, Sintesis dan Karakterisasi Pigmen Merah Hematit (α -Fe₂O₃) dari Pasir Besi Kabupaten Sijunjung, Sumatera Barat, Indonesia, *Periodic*, 12, 1, (2023), 9-13 <https://doi.org/10.24036/p.v12i1.115856>
- [4] Mastuki Mastuki, A. W. Brata, A. G. Istiawan, B. Aditya, H. Masrufi, Study Experimental The Effect of CaCO₃ and Fe₂O₃ Mass Composition Ratio on Calcium Ferrite Phase Formation Base on Local Materials Iron Sand and Limestone, *SINTEK JURNAL: Jurnal Ilmiah Teknik Mesin*, 14, 1, (2020), 27-31 <https://doi.org/10.24853/sintek.14.1.27-31>
- [5] Jingyi Wang, Panpan Sun, Huimin Xue, Jinxiu Chen, Heng Zhang, Wancheng Zhu, Red mud derived facile hydrothermal synthesis of hierarchical porous α -Fe₂O₃ microspheres as efficient adsorbents for removal of Congo red, *Journal of Physics and Chemistry of Solids*, 140, (2020), 109379 <https://doi.org/10.1016/j.jpcs.2020.109379>
- [6] Zahra Karimi, Ahmad Rahbar-Kelishami, Efficient utilization of red mud waste via stepwise leaching to obtain α -hematite and mesoporous γ -alumina, *Scientific Reports*, 13, 1, (2023), 8527 <https://doi.org/10.1038/s41598-023-35753-w>
- [7] Indi Rizki Wahyinto, Anthoni B. Aritonang, Titin Anita Zaharah, Extraction and Characterization of Fe₂O₃ from Red Mud PT. Indonesia Chemical Alumina West Kalimantan, *Berkala Sainstek*, 10, 3, (2022), 155-161 <https://doi.org/10.19184/bst.v10i3.30252>
- [8] Pratibha Sharma, Sujata Kumari, Debasree Ghosh, Vandana Yadav, Ankush Vij, Pooja Rawat, Shalendra Kumar, Chittaranjan Sinha, Sonia Saini, Vivek Sharma, Md Imtaiyaz Hassan, Chandra Mohan Srivastava, Sudip Majumder, Capping agent-induced variation of physicochemical and biological properties of α -Fe₂O₃ nanoparticles, *Materials Chemistry and Physics*, 258, (2021), 123899 <https://doi.org/10.1016/j.matchemphys.2020.123899>
- [9] Namra Abid, Aqib Muhammad Khan, Sara Shujait, Kainat Chaudhary, Muhammad Ikram, Muhammad Imran, Junaid Haider, Maaz Khan, Qasim Khan, Muhammad Maqbool, Synthesis of nanomaterials using various top-down and bottom-up approaches, influencing factors, advantages, and disadvantages: A review, *Advances in Colloid and Interface Science*, 300, (2022), 102597 <https://doi.org/10.1016/j.cis.2021.102597>
- [10] Rabia Javed, Muhammad Zia, Sania Naz, Samson O. Aisida, Noor ul Ain, Qiang Ao, Role of capping agents

- in the application of nanoparticles in biomedicine and environmental remediation: recent trends and future prospects, *Journal of Nanobiotechnology*, 18, 1, (2020), 172 <https://doi.org/10.1186/s12951-020-00704-4>
- [11] Vidya Devadiga, Geetha M. Pinto, Ronald Nazareth, K. Amrutha, Synthesis of functionalized α -Fe₂O₃ nanoparticles: Characterization and applications, *Materials Today: Proceedings*, (2023), <https://doi.org/10.1016/j.matpr.2023.05.111>
- [12] Berlian Sitorus, Mincen Reva, Intan Syahbanu, Extraction of Scandium and Removal of Iron from Bauxite Residue using Hydrochloric Acid Solution with/without Addition of EDTA, *Reaktor*, 24, 3, (2025), 76-81 <https://doi.org/10.14710/reaktor.24.3.76-81>
- [13] Pratishtha Kushwaha, Pratima Chauhan, Synthesis of spherical and Rod-Like EDTA assisted α -Fe₂O₃ nanoparticles via Co-precipitation method, *Materials Today: Proceedings*, 44, (2021), 3086-3090 <https://doi.org/10.1016/j.matpr.2021.02.450>
- [14] Titin Anita Zaharah, Wanda Rossalina, Imelda Hotmarisi Silalahi, Komposisi Unsur dan Karakterisasi Mineral Magnetik dalam Red Mud, Residu Bauksit di PT. Indonesia Chemical Alumina (ICA) Kalimantan Barat (*Elemental Composition And Mineral Characteristics of Magnetic Red Mud, Bauxite Residue at PT. Indonesia Chemical Alumina (ICA), West Kalimantan*), *Indonesian Journal of Pure and Applied Chemistry*, 4, 3, (2021), 139-144 <https://doi.org/10.26418/indonesian.v4i3.49660>
- [15] G. Svehla, *Vogel's Textbook of Macro and Semimicro Qualitative Inorganic Analysis*, Longman, 1985,
- [16] Yong Richard Sriwijaya, Paramita Jaya Ratri, Tirta Rona Mayangsari, Azis Adharis, Shabrina Sri Riswati, Synthesis of Iron Oxide (Fe₂O₃)-Xanthan Gum Nanoparticle Composites Its Potential as a Chemical Flooding Media in Enhanced Oil Recovery (EOR), *Jurnal Kimia Valensi*, 9, 1, (2023), 53-58 <https://doi.org/10.15408/jkv.v9i1.29468>
- [17] V. Archana, J. Joseph Prince, S. Kalainathan, Simple One-Step Leaf Extract-Assisted Preparation of α -Fe₂O₃ Nanoparticles, Physicochemical Properties, and Its Sunlight-Driven Photocatalytic Activity on Methylene Blue Dye Degradation, *Journal of Nanomaterials*, 2021, 1, (2021), 8570351 <https://doi.org/10.1155/2021/8570351>
- [18] Pantharee Kongsat, Kobkun Kudkaew, Jiratikul Tangjai, Edgar A. O'Rear, Thirawudh Pongprayoon, Synthesis of structure-controlled hematite nanoparticles by a surfactant-assisted hydrothermal method and property analysis, *Journal of Physics and Chemistry of Solids*, 148, (2021), 109685 <https://doi.org/10.1016/j.jpcs.2020.109685>
- [19] Hikaru Sawai, Ismail M. M. Rahman, Mayuko Fujita, Naoyuki Jii, Tomoya Wakabayashi, Zinnat A. Begum, Teruya Maki, Satoshi Mizutani, Hiroshi Hasegawa, Decontamination of metal-contaminated waste foundry sands using an EDTA-NaOH-NH₃ washing solution, *Chemical Engineering Journal*, 296, (2016), 199-208 <https://doi.org/10.1016/j.cej.2016.03.078>
- [20] Amanda Kulpa, Jacek Ryl, Grzegorz Skowierzak, Adrian Koterwa, Grzegorz Schroeder, Tadeusz Ossowski, Paweł Niedziałkowski, Comparison of Cadmium Cd²⁺ and Lead Pb²⁺ Binding by Fe₂O₃@SiO₂-EDTA Nanoparticles – Binding Stability and Kinetic Studies, *Electroanalysis*, 32, 3, (2020), 588-597 <https://doi.org/10.1002/elan.201900616>
- [21] A. G. Magdalena, I. M. B. Silva, R. F. C. Marques, A. R. F. Pipi, P. N. Lisboa-Filho, M. Jafelicci, EDTA-functionalized Fe₃O₄ nanoparticles, *Journal of Physics and Chemistry of Solids*, 113, (2018), 5-10 <https://doi.org/10.1016/j.jpcs.2017.10.002>
- [22] Eduwin Saputra, A colorimetric detection of creatinine based-on EDTA capped-gold nanoparticles (EDTA-AuNPs): Digital Image Colorimetry, *Sensors International*, 5, (2024), 100286 <https://doi.org/10.1016/j.sintl.2024.100286>
- [23] Maryam Jouyandeh, Mohammad Reza Ganjali, Jagar A. Ali, Mustafa Aghazadeh, Isa Karimzadeh, Krzysztof Formela, Xavier Colom, Javier Cañavate, Mohammad Reza Saeb, Curing epoxy with ethylenediaminetetraacetic acid (EDTA) surface-functionalized Co_xFe_{3-x}O₄ magnetic nanoparticles, *Progress in Organic Coatings*, 136, (2019), 105248 <https://doi.org/10.1016/j.porgcoat.2019.105248>
- [24] Ekta Shah, Pratik Upadhyay, Mala Singh, Mohmmad Shoab Mansuri, Rasheedunnisa Begum, Navin Sheth, Hemant P. Soni, EDTA capped iron oxide nanoparticles magnetic micelles: drug delivery vehicle for treatment of chronic myeloid leukemia and T₁-T₂ dual contrast agent for magnetic resonance imaging, *New Journal of Chemistry*, 40, 11, (2016), 9507-9519 <https://doi.org/10.1039/c6nj00655h>
- [25] Abdenacer Benhammada, Djalal Trache, Mohamed Kesraoui, Ahmed Fouzi Tarchoun, Salim Chelouche, Abderrahmane Mezroua, Synthesis and characterization of α -Fe₂O₃ nanoparticles from different precursors and their catalytic effect on the thermal decomposition of nitrocellulose, *Thermochimica Acta*, 686, (2020), 178570 <https://doi.org/10.1016/j.tca.2020.178570>
- [26] Daa Eldin Fouad, Chunhong Zhang, Hamdy El-Didamony, Liu Yingnan, Tadele Daniel Mekuria, Ahmer Hussain Shah, Improved size, morphology and crystallinity of hematite (α -Fe₂O₃) nanoparticles synthesized via the precipitation route using ferric sulfate precursor, *Results in Physics*, 12, (2019), 1253-1261 <https://doi.org/10.1016/j.rinp.2019.01.005>
- [27] Camilah D. Powell, Amanda W. Lounsbury, Zachary S. Fishman, Christian L. Coonrod, Miranda J. Gallagher, Dino Villagran, Julie B. Zimmerman, Lisa D. Pfefferle, Michael S. Wong, Nano-structural effects on Hematite (α -Fe₂O₃) nanoparticle radiofrequency heating, *Nano Convergence*, 8, 1, (2021), 8 <https://doi.org/10.1186/s40580-021-00258-7>
- [28] Adwitiya Chakraborty, Prasanta Kumar Sinha, Milan Kanti Naskar, Low Temperature Processing of Iron Oxide Nanoflakes from Red Mud Extract toward Favorable De-arsenification of Water, *ACS Omega*, 8, 32, (2023), 29281-29291 <https://doi.org/10.1021/acsomega.3c02689>
- [29] Thandi B. Mbuyazi, Peter A. Ajibade, Influence of Different Capping Agents on the Structural, Optical, and Photocatalytic Degradation Efficiency of Magnetite (Fe₃O₄) Nanoparticles, *Nanomaterials*, 13, 14, (2023), 2067 <https://doi.org/10.3390/nano13142067>